Modeling the Effects of the PCB Motion on the Response of Microstructures under Mechanical Shock

Abdallah H Ramini, Mohammad I Younis, and Ronald Miles
Department of Mechanical Engineering
State University of New York at Binghamton
Binghamton, NY, 13902
myounis@binghamton.edu

Abstract

Microelectomechanical systems (MEMS) are often used in portable electronic products that can be subjected to mechanical shock or impact due to being dropped accidentally. This work presents a modeling and simulation effort to investigate the effect of the vibration of a printed circuit board (PCB) on the dynamics of MEMS microstructures when subjected to shock. Two models are presented. In the first approach, the PCB is modeled as an Euler-Bernoulli beam to which a lumped model of a MEMS device is attached. In the second approach, a special case of a cantilever microbeam is modeled as a distributed-parameter system, which is attached to the PCB. These lumped-distributed and distributed-distributed models are solved numerically by integration of the equation of motion over time using the Galerkin procedure. Results of the two models are compared against each other for the case of a cantilever microbeam and also compared to the predictions of a finite-element model using ANSYS. The influence of the higher order vibration modes of the PCB, the location of the MEMS device on the PCB, the electrostatic forces, damping, and shock pulse duration are presented. It is found that neglecting the effects of the higher order modes of the PCB and the location of the MEMS device can cause incorrect predictions of the response of the microstructure and may lead to failure of the MEMS device. It is observed from the results that in some cases, depending on the different parameters of the problem, the response of the microstructure can be amplified causing early dynamic pull-in and hence possibly failure of the device.

Index Terms—Printed Circuit Board, Mechanical Shock, Vibrations, Electrostatic Force, Pull-in.

1. Introduction

A new challenge in the development of MEMS technology is the ability of MEMS devices to perform and maintain their functions in hostile vibration and shock environments. Without sufficient attention on these factors, reliability and quality of MEMS devices can be weakened making them unusable or even destroyed at the moment of fabrication. MEMS can be exposed to shock during fabrication, storage, and while in use. Shock can cause several failure modes of microstructures, such as mechanical failure, stiction, and short circuits.

A current trend in the electronics and MEMS industries is to manufacture thin and flexible Printed Circuit Boards (PCB). Hence, PCBs can undergo large motion when subjected to mechanical shock or vibration. This motion can be transferred to the microstructure leading to either its failure or malfunction. The interaction of the vibration modes of the PCB with that of microstructures can also lead to resonant behaviors leading to violent motions and unaccounted for consequences. Other sources of significant effects on the motion of a microstructure are electrostatic forces in MEMS devices. These, combined with mechanical shock, can lead to early dynamic pull-in instability of the microstructures. Thus, understanding the interaction of mechanical shock, electrostatic forces, and the motion of PCB with that of microstructures is necessary to ensure safe and reliable operation of MEMS devices.

A number of investigations have been conducted in recent years to investigate mechanical shock in MEMS [1-9]. Comprehensive reviews of these can be found in [10-16]. Among the recent contributions, Kimberley *et al.* investigated experimentally the dynamic failure of gold clamped-clamped microbeams using three different experimental setups: a drop weight tower, a Hopkinson pressure bar and a pulsed laser loading technique [8]. Sheey *et al.* investigated the failure mechanisms of single crystal silicon microcantilever devices under high-g accelerations using a modified Hopkinson pressure bar [9].

One can note that inadequate attention has been addressed to the possible coupling between the vibrations of the PCB and the microstructures mounted on top of it. Particularly, the possibility of interaction among the higher order-modes of the PCB and the natural frequencies of the microstructures (especially the lowest ones) have not been investigated before in great depth. Moreover, the effect of the location of the MEMS chip over the PCB has not been given adequate attention. Investigating these issues represents the major objective of this paper.

In previous works, we investigated the response of microstructures under the combined effects of mechanical shock and electrostatic forces [10-12]. Computationally efficient approaches to study shock in MEMS were presented in [13]. We also studied the effect of the PCB motion on the response of a microstructure theoretically using a two-degree-of-

978-1-4244-7027-310/$26.00 ©2010 IEEE —*1*—

11th. Int. Conf. on Thermal, Mechanical and Multiphysics Simulation and Experiments in Micro-Electronics and Micro-Systems, EuroSimE 2010

freedom model and also experimentally [14, 15]. A continuous model of a microbeam coupled to a spring-mass-damper model of a PCB was also presented in [14, 15]. The response of electrically actuated resonators to mechanical shock was analyzed in [16].

The objective of this work is to investigate the effect of the interaction of higher order modes of the PCB with the response of the microstructures under mechanical shock. A second objective is to study the effect of the location of the microstructure on the PCB. Towards this end, we present a precise dynamical model for the mechanical shock problem on the PCB. Here, the mechanical shock is modeled as a base-excitation acceleration pulse affecting the PCB-MEMS assembly. A comparison between this case and an ANSYS finite element model is made. Simulation results showing the effects of different PCB lengths on the response of MEMS devices under base excitation shock loads will be presented.

2. Problem Formulation

Two approaches will be presented: beam-lumped model and beam-beam model. In both approaches, the PCB is treated as an Euler-Bernoulli beam. The first approach (beam-lumped model) aims to model a generic microstructure attached to the PCB. In this case, a lumped spring-mass-damper model is used to represent the motion of the microstructure. The second approach (beam-beam model) represents a more accurate model that is specially developed for cantilever microbeams, which are commonly used in MEMS. While the second approach is more accurate to model cantilever microbeams, since it counts for its distribution of mass and stiffness and enable accurate modeling for other surface forces such as electrostatic forces; it is limited to cantilevers only.

In this paper, we study the case when the shock load is assumed to be a base-excitation acceleration pulse, which occurs when the base of the assembly undergoes a sudden acceleration change. This happens, for example, due to the drop of the assembly to the ground or due to a drop-table test. To model a shock pulse due to a drop test, the pulse is assumed to be a half-sine acceleration pulse of amplitude A_o and period T_{shock}, as shown in Figure 1.
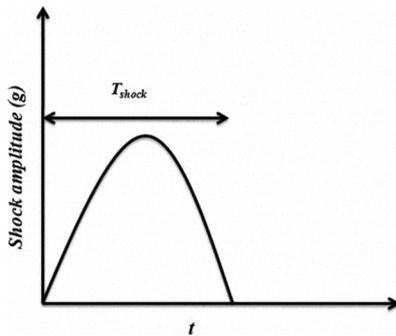
Figure 1: A schematic of a half-sine pulse used to model actual shock loads, base shock acceleration.

The base-excitation acceleration $\ddot{y}$ is expressed as,

$$\ddot{y} = A_o \begin{bmatrix} \sin(\omega_{pulse}t)u(t) \\ +\sin(\omega_{pulse}(t-T_{shock}))u(t-T_{shock}) \end{bmatrix}$$

(1)

where $\ddot{y}$ is the base –excitation acceleration, ω_{pulse} is the pulse frequency, t is time, and $u(t)$ is the unit step function.
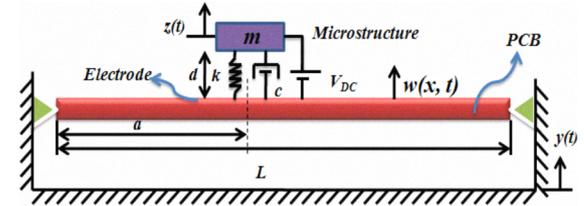
2.1. Beam-lumped model

Figure 2: A schematic diagram for the beam-lumped model.

Figure 2 shows the beam-lumped model. In the figure, $w(x,t)$ refers to the PCB motion, such as a beam or a plate, with respect to $y(t)$ which is the input base displacement, and $z(t)$ represents the motion of the microstructure relative to $w(x,t)$. The rest of the model parameters are as shown in Figure 2 and as defined in Table 1. To consider a generic form of the MEMS devices, the microstructure is assumed to be actuated by a parallel plate electrostatic force. Hence, the microstructure forms an upper electrode located at a distance d above the substrate as shown in Figure 2.

Using Hamilton's principle, the equations of motion that govern the transverse deflection of the PCB $w(x,t)$ and the microstructure motion $z(t)$ are written, respectively, as,

$$\rho_{PCB}BH\ddot{w} + E_{PCB}I_{PCB}w_{xxxx} + c_{PCB}\dot{w} = -\rho_{PCB}BH\ddot{y}$$

(2)

$$m\ddot{z}(t) + kz(t) + c\dot{z}(t) = -m\left[\ddot{y}(t) + \ddot{w}(a,t)\right]$$

$$+\frac{\varepsilon A V_{DC}^2}{2\left[d - z(t) + w(a,t)\right]^2}$$

(3)

where the subscript represents partial differentiation.

Here, (2) and (3) are used to model the influence of the PCB motion on the response of a microstructure of arbitrary shape. Equation (2) is solved analytically using the assumed-modes method [17]. Then, the resulting nonlinear equation is substituted for $w(a,t)$ into (3). The result is then integrated numerically using the Runge-Kutta method.

—2—

Table 1: A summary of the design variables and definitions required for the analysis of the two used models. (The numerical values of some of the listed parameters are used for the case study.)

Symbol	Quantity
$w(x,t)$	The motion of the PCB, as measured with respect to the input base-displacement $y(t)$.
$z(t)$	The motion of the MEMS.
$y(t)$	The input base-displacement.
d	The capacitor gap width= $2\ \mu m$.
V_{DC}	The DC polarization voltage.
L	The PCB Length.
B	The width of the PCB ($B=L/2$).
H	The thickness of the PCB= $500\ \mu m$.
E_{PCB}	The Young's modulus of the PCB= 25 GPa.
I_{PCB}	The area moment of inertia for the PCB.
ρ_{PCB}	The density of the PCB = $3200\ kg.m^{-3}$.
c_{PCB}	The modal damping coefficient of the PCB.
m	The mass of the microstructure.
k	The stiffness of the microstructure.
c	The damping of the microstructure.
a	The position of the microstructure over the PCB.
t	Time in seconds or milliseconds.
T_{MEMS}	The natural period of the microstructure or the microbeam.
ε	The dielectric constant of the gap medium= $8.86\times 10^{-12}F.m^{-1}$.
A	The electrode area of the microstructure.
ω_{pulse}	The shock pulse frequency.
T_{shock}	The shock duration (half-sine wave).
T_{PCB}	The natural period of the PCB.
fn_1	The 1st natural frequency of the PCB.
fn_2	The 2nd natural frequency of the PCB.
fn_3	The 3rd natural frequency of the PCB.
fn_4	The 4th natural frequency of the PCB.

2.2. Beam-beam model
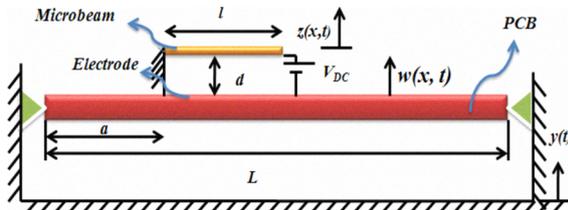
Figure 3: A schematic diagram for the beam-beam model.

Figure 3 shows the beam-beam model, which is geared to model the cantilever microbeam as a special case. Here $w(x,t)$ represents the PCB motion with respect to $y(t)$ and $z(x,t)$ represents the motion of the microstructure, relative to the PCB motion .

Using Hamilton's principle, the transverse deflection of the PCB $w(x,t)$ and the microstructure motion $z(x,t)$ are written, respectively, as,

$$\rho_{PCB}BH\ddot{w}+E_{PCB}I_{PCB}w_{xxxx}+c_{PCB}\dot{w}=-\rho_{PCB}BH\ddot{y} \quad (4)$$

$$\rho_{MEMS}bh\ddot{z}(x,t)+E_{MEMS}I_{MEMS}z_{xxxx}(t)+c_{MEMS}\dot{z}(x,t)$$

$$=-\rho_{MEMS}bh\left[\ddot{y}(t)+\ddot{w}(a,t)\right]+\frac{\varepsilon blV_{DC}^2}{2[d-z(x,t)+w(a,t)]^2} \quad (5)$$

Here, (4) and (5) are used to model the influence of the PCB motion on the response of a cantilever microbeam. Equation (4) is solved analytically using the assumed-modes method [17]. Then, $w(a,t)$ and $\ddot{w}(a,t)$ are calculated and substituted into (5). The resulting nonlinear equation is solved using reduced-order model based on Galerkin method [18]. Then it is integrated numerically using the Runge-Kutta method. This yields a finite-degree-of-freedom system consisting of ordinary-differential equations in time. The linear mode shapes of the straight microbeam and PCB are used as basis functions in the Galerkin procedure. The even modes are not included in the solution for the PCB motion since they are antisymmetric modes and hence their influence on the microbeam dynamics is negligible. The resulting ordinary differential equations are integrated numerically with respect to time using the Runge-Kutta method.

Table 2: A summary of all design variables and definitions required for cantilever microbeam.

Symbol	Quantity
l	The microbeam length = $400\ \mu m$.
b	The microbeam width = $50\ \mu m$.
h	The microbeam thickness = $1\ \mu m$.
I_{MEMS}	The area moment of inertia for the microbeam.
E_{MEMS}	The microbeam's Young's modulus = 169 GPa.
ρ_{MEMS}	The density of the Polysilicon = 2332 $kg.m^{-3}$.
c_{MEMS}	The modal damping of the microbeam.
T_{MEMS}	The natural period of the microbeam (in this case cantilever microbeam).
f_{beam}	The 1st natural frequency of the cantilever microbeam = $8.6\ kHz$.

2.3. A comparison between two models

As a case study, we consider a cantilever microbeam with the parameters of Table 2. For

comparison purposes between the two models, a shock load of amplitude *200 g* assumed as an input for the two models. The assumed parameters of the PCB are *L=10 cm, B=5 cm* and *H=500 μm*. The position of the microbeam is assumed to be at the middle of the PCB (*a=L/2*). No electrostatic forces are assumed in this case.

To use the beam-lumped model, an effective mass m_{eff} and stiffness coefficient k of the cantilever beam, need to be calculated as,

$$k = \frac{8E_{MEMS}I_{MEMS}}{l^3} \quad (6)$$

$$m_{eff} = \frac{8E_{MEMS}I_{MEMS}}{l^3} \quad (7)$$

where

$$\omega_1^2 = \frac{3.52^2 E_{MEMS}I_{MEMS}}{l^3 m} \quad (8)$$

Note that m_{eff} will replace the mass coefficient m of $\ddot{z}(t)$ in (3) only in the left-hand side and not the one on the right-hand side of (3) (the coefficient of $\ddot{y}(t) + \ddot{w}(a,t)$). Since m is the coefficient of the force distributed over the length of the microbeam. Next we normalize the resulting equation by dividing by m_{eff}, which yields

$$\ddot{z}(t) + \omega_1^2 z(t) + 2\zeta\omega_1\dot{z}(t) = -1.548\left[\ddot{y}(t) + \ddot{w}(a,t)\right] \quad (9)$$

where ζ is the damping ratio, which is assumed to be $\zeta = 0.001$. Also, we assume the same value as the modal damping ratio for the microbeam in the beam-beam model. This value will be adapted throughout the paper. Evaluating the above expressions for the dimensions of the microbeam yields $m_{eff}=3.0129\times 10^{-11}$ kg and $k=0.088$ N.m^{-1}. Next, we compare the results using (9) and those using (4) and (5), as explained in Section *2.2*.

In Figure 4, it can be noticed that the microbeam response in the two models is the same. The beam-lumped model is generic and it can be used for MEMS devices with irregular shapes. The beam-beam model is more specific for a cantilever microbeam attached to PCB, which is used commonly in MEMS. Throughout the remainder of the paper, we will focus on the cantilever microbeam as a case study and use the beam-beam model.

3. The Analytical Model versus FE Model

In this section, we use the finite element (FE) software ANSYS to validate the results of the analytical model. A 2-D 8-node element (SHELL63) and a 2-D 6-node element (BEAM4) are used to model the PCB with the microbeam. The shock is applied to all the nodes on the model via the "ACEL" command

using discrete data points during a transient dynamic analysis. The assumed parameters of the PCB are *L=10 cm, B=5 cm* and *H=500 μm*. The position of the microbeam is assumed to be at the middle of the PCB (*a=L/2*). No electrostatic forces are assumed in this case, as well.
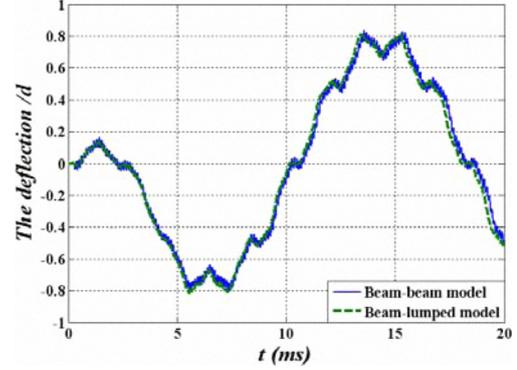

Figure 4: A comparison between the beam-beam model and the beam-lumped model for the case study (cantilever beam), when subjected to shock of amplitude=200 g with T_{shock} = 5 ms.
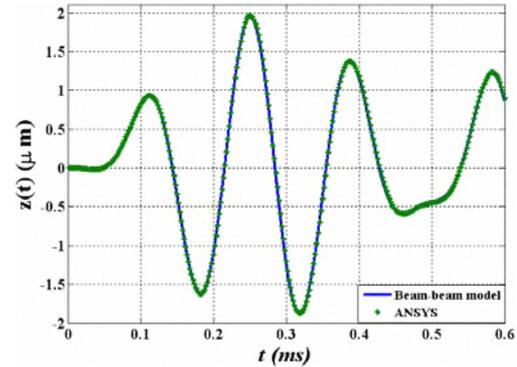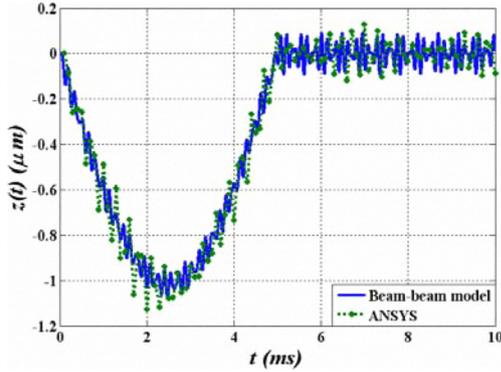

Figure 5: The response of a cantilever beam, placed at the center of the PCB (a=L/2), generated using the dynamic FE model (*), the beam-beam model (solid), when T_{shock} = 0.1 ms and shock of amplitude=50 g for f_{beam} =8.6 kHz and fn_1 = 64Hz.

Figure 5 shows a comparison between the results of the beam-beam model (*solid*) and the FE model results (***) for a shock pulse of T_{shock} =0.1 ms and amplitude *50 g*. Note here, that the first natural frequency of the PCB fn_1=64 Hz and the natural frequency of the microbeam f_{beam}=8.6 kHz. Also the shock frequency $1/T_{shock}$=10 kHz. Since the ratio between the shock frequency and f_{beam} equals *1.16*, this means that the shock pulse is in the dynamic regime on the shock-response spectrum [13]. It is clear that using the beam-beam model for this range of shock amplitude yields accurate results. It can be concluded from Figure 5 that the microbeam is likely to hit the substrate for shock load exceeding *50*

g. Such an impact can lead to a failure in the cantilever microbeam.

Figure 6 shows a comparison between the results of the beam-beam model (*solid*) and the FE model results (***) when shock pulse of $T_{shock}= 5$ *ms* and amplitude *200 g*. Here, the shock frequency *$1/T_{shock}=200$ Hz*. Since the ratio between the shock frequency and f_{beam} equals *43*, this means that shock pulse is in the quasi-static regime [13]. Also, it is clear that using the beam-beam model for this range yields accurate results as well.

Figure 6: The response of a cantilever beam, placed at the center of the PCB a=L/2), generated using the dynamic FE model (*), the beam-beam model (solid), when T_{shock} = 5 ms and shock amplitude=200 g for f_{beam} =8.6 kHz and fn_1 = 64 Hz.
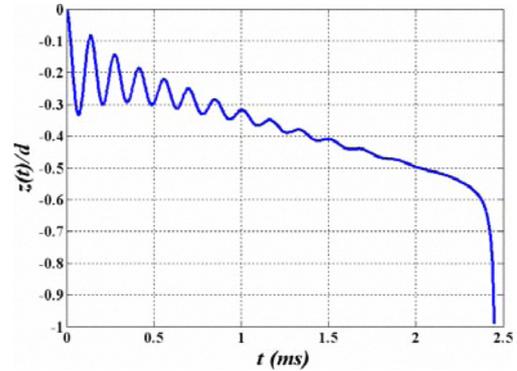
4. The Effect of Electrostatic Force and the PCB Motion

Here, we study the combined effect of the PCB motion and the electrostatic forces on the response of a cantilever microbeam to shock load. Again, we use the beam-beam mode.

First, we consider the response due to each force alone. The assumed parameters of the PCB are *L=10 cm*, *B=5 cm* and *H=500 μm*. In Figure 7a, the response of the microbeam under the electrostatic load only ($V_{DC}=1.04$ V) is shown. As noted, the beam doesn't hit the substrate and it settles to a stable position. Figure 7b shows the microbeam's response under shock of amplitude *70 g* only. Also in this case, the microbeam doesn't hit the substrate. The response doesn't reach the gap neither under shock amplitude *70 g* nor under the electrostatic load $V_{DC}=1.04$ V. However, if both the shock and the electrostatic load are applied on the microbeam at the same time, the microbeam reaches the dynamic pull-in instability and hits the substrate [10-12].

(a)

(b)
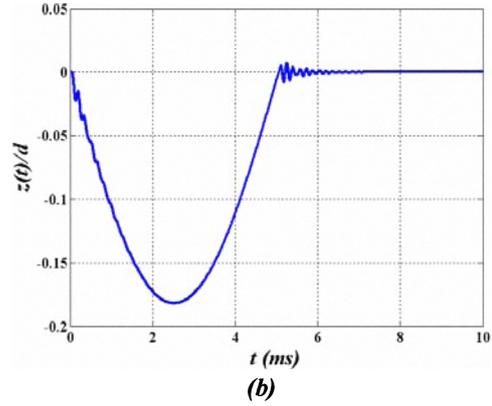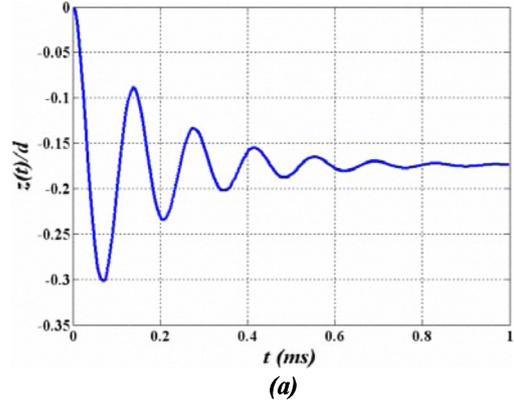
Figure 7: (a) The response of the microbeam under electrostatic load only with V_{DC} =1.04 V. (b) The response of the microbeam under shock only of amplitude 70 g and T_{shock}=5 ms.

Figure 8: The response of the combined effect of the shock and the electrostatic forces showing dynamic pull-in.

Figure 8 shows clearly the dynamic pull-in instability. We should point out here the fact that the electrostatic force has a softening effect that decreases the natural frequency of the microbeam until it reaches zero at pull-in [18, 19].

Next, we investigate the effect of varying the shock

duration T_{shock}. So, we show in Figure 9 the pull-in voltage versus the shock amplitude for various values of T_{shock}. The length is adjusted to $L= 1.54$ cm and the rest of the parameters are in Table 1 and Table 2, such that the first natural frequency of the PCB (fn_1) is away from f_{beam} ($T_{PCB}=5.8$ T_{MEMS} and the second natural period of the PCB=0.5 T_{MEMS}). It is clear from Figure 9 that the lowest pull-in voltage threshold occurs when $T_{shock}=3.6$ T_{MEMS}. Here, one can note that neglecting the effect of the PCB motion (case of $T_{shock}=$ T_{MEMS}) underestimates the pull-in instability.

It is worth mentioning that, under the straight horizontal line in Figure 9, the shock effect becomes so dominant that it is hard to get a clear distinction between pull-in and collapse due to shock. This might be due to fractal dynamic behavior of the nonlinear system [10, 20].
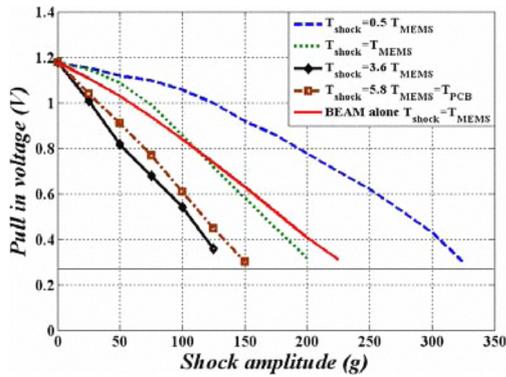

Figure 9: The pull-in voltage versus the shock amplitude when f_{beam} =8.6 kHz and fn_1 = 2.8 kHz.

To explain the results of Figure 9, we show the shock-response spectrum of the microbeam in Figure 10. It can be noticed that the maximum response amplitude occurs at $T_{shock}=3.6T_{MEMS}=0.7T_{PCB}$. The maximum deflection for the PCB occurs when $T_{shock}=0.7$ T_{PCB}, which justifies why the maximum deflection for the microbeam occurs at $T_{shock}=3.6$ T_{MEMS} (the PCB response is the maximum in the dynamic regime on the shock-response spectrum for the PCB [13]). Also, one can note from Figure 9 that the curve $T_{shock}=$ T_{MEMS} assuming a beam model alone switches and crosses the curve of $T_{shock}=$ T_{MEMS} including the effect of the PCB motion. This is due to the softening effect of the electrostatic force, which increases T_{MEMS}, thereby changing the ratio $T_{MEMS}/$ T_{PCB}.

To clarify further the meaning of these results, the microbeam response is shown for two cases with and without the dynamic pull-in. In Figure 11a, the microbeam response reaches the dynamic pull-in where it is not attached to a PCB. In Figure 11b, if we assume the microbeam attached to a PCB of $fn_1=2.8$ kHz, then f_{beam} /fn_1 = 3.7. Hence, the PCB attenuates the microbeam response preventing pull-in.

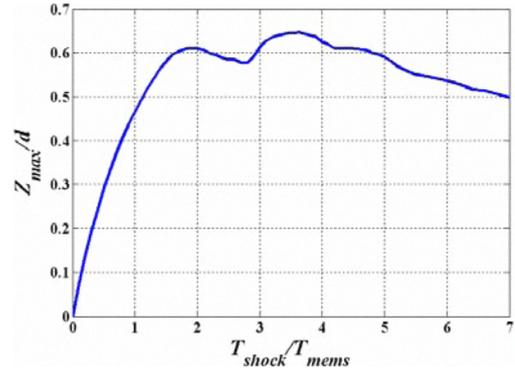Figure 10: Shock-response spectrum of the microbeam including the PCB effect when f_{beam} =8.6 kHz and fn_1 = 2.8 kHz under shock amplitude 100 g.

(a)
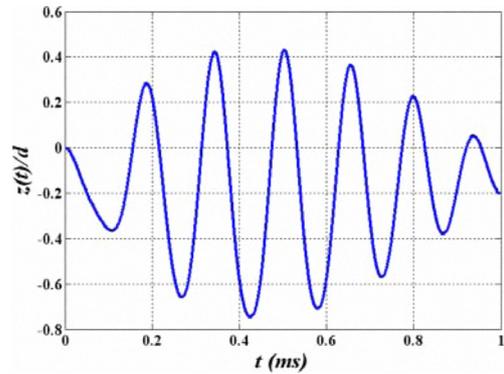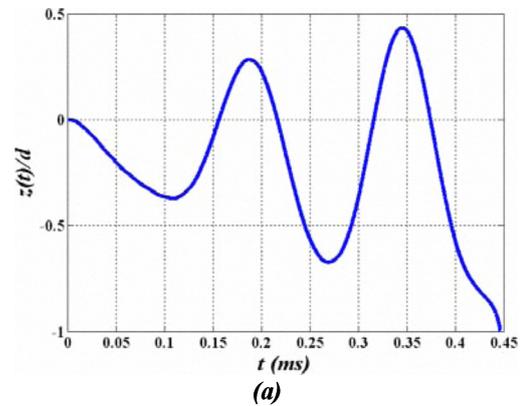

Figure 11: (a) The microbeam response under V_{DC}=1.04 V and shock pulse of amplitude 50 g and T_{shock} =T_{MEMS} without the PCB effect. (b) The microbeam response under V_{DC}=1.04 V and shock pulse of amplitude 50 g and T_{shock} =T_{MEMS} with the PCB effect. The modal damping for the microbeam is assumed=0.001.

In order to clarify that the case of $T_{shock}=T_{MEMS}=T_{PCB}$ is the most severe case. Figure 13 shows the shock-response spectrum for the microbeam. It can be noticed that the maximum response amplitude

—6—

occurs at $T_{shock}=T_{MEMS}=T_{PCB}$.
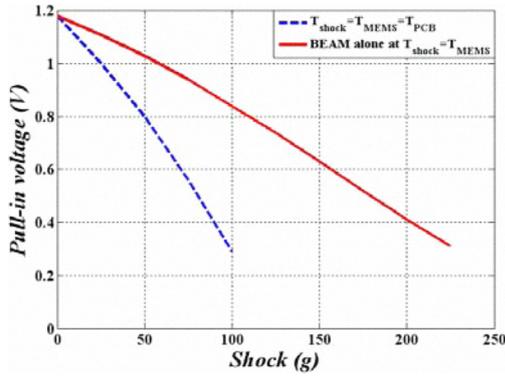
Figure 12: The pull-in voltage versus the shock amplitude when the natural frequency of the microbeam and the PCB natural frequency =8.6 kHz.
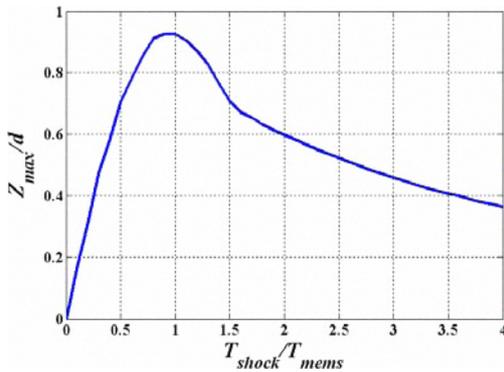
Figure 13: Shock spectrum of the microbeam including the PCB effect when $f_{beam}=fn_1=$ 8.6 kHz under shock amplitude 100 g.

The results indicate the importance of modeling the effect of the PCB motion with the electrostatic forces. By ignoring the effect of the PCB, there is a risk that the MEMS device fails to function appropriately and it might fail mechanically or electrically. On the other hand, the natural frequency of the PCB can be used to tune the shock-pull-in curve for its use as a switch triggered by mechanical shock [10-12].

5. The Effect of the Microbeam Position and the Higher-Order Modes of the PCB

In this section, we investigate the effects of the position of the microbeam and the interaction of its higher-order modes with the fundamental mode of the microbeam.

The length of the PCB is taken to be ($L=0.85$ cm), such that $fn_1= f_{beam}$. Next we vary T_{shock} such that it matches one of the natural frequencies of the PCB. In the first case, ($1/T_{shock}= fn_1=f_{beam}$). As shown in Figure 14, the maximum deflection occurs when the

microbeam is mounted at the middle of the PCB. The same conclusion is noted when the shock duration is varied such that $1/T_{shock}= fn_2$ or $1/T_{shock}= fn_3$. However, the amplitude response of the case of $1/T_{shock}= fn_1$ is the most significant.
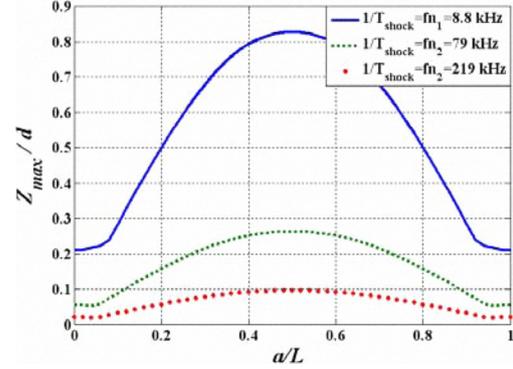
Figure 14: The maximum displacement of the cantilever beam when subjected to shock amplitude 50 g with $f_{beam}\approx fn_1=8.8$ kHz. The PCB's natural frequencies are $fn_1= 8.8$ kHz, $fn_2=79$ kHz, and $fn_3=219$ kHz.

Next, we study the case when the natural period of the microbeam T_{MEMS} matches the 2nd natural period of the PCB ($1/fn_2$) and T_{shock}. Hence, L is changed to $L=2.5$ cm. In Figure 15, the maximum deflection occurs when the shock duration gets close to the second natural period of the PCB or ($1/T_{shock}= fn_2$).
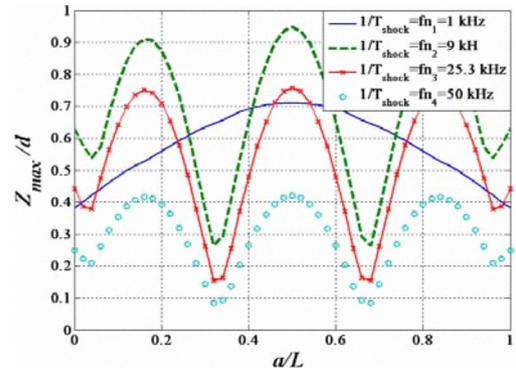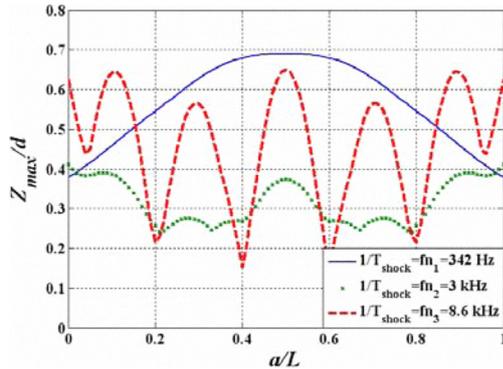

Figure 15: The maximum displacement of the cantilever beam when subjected to shock amplitude 150 g with $f_{beam}\approx fn_2$. The PCB's natural frequencies are $fn_1=1$ kHz, $fn_2=9$ kHz, $fn_3=25.3$ kHz, and $fn_4=50$ kHz.

Note that, in this case, matching the first natural period of the PCB and T_{shock} is not as significant as the case of ($1/T_{shock}= fn_2$). Also, note that the response on the case of $1/T_{shock}= fn_3$ is also more significant than $1/T_{shock}= fn_1$. This indicates the importance of accounting for the higher-order modes of the PCB, which are assumed negligible. One final observation

—7—

that can be drawn from Figure 15 is that there are several locations on the PCB where the response can be large, and not only at the middle of the PCB as traditionally is assumed.

In Figure 16, we change the length of the PCB to $L=4.3$ cm such that $fn_3 = f_{beam}$. One can conclude that the 1st mode of the PCB starts to dominate the response when $f_{beam} >> fn_1$ or fn_2. However, it is noted that when $1/T_{shock} = fn_3$, the response becomes significant at the third mode. Hence several locations on the PCB result in significant response of the microbeam.

Figure 16: The maximum displacement of the cantilever beam when subjected shock amplitude 150 g with $f_{beam} = fn_3 = 8.6$ kHz. The PCB's natural frequencies are $fn_1 = 342$ Hz, $fn_2 = 3$ kHz, and $fn_3 = 8.6$ kHz.

In summary, we conclude that the higher order modes of vibration of a microbeam may contribute to its response in other cases than when one of those modes has a natural frequency that is near the natural frequency of the PCB and the shock pulse frequency.

6. Conclusions

A beam-beam model for both the microstructure and the PCB (continuous model for the microbeam with continuous model for the PCB) was used to investigate the effect of higher-order modes of the PCB when they interact with the fundamental natural frequency of a microstructure of MEMS device. It was found that higher modes of the PCB can have significant effects on the MEMS device response, especially for the cases when the natural frequency of the MEMS is near both the natural frequency of the PCB and the shock pulse frequency. By ignoring the effects of the PCB and the higher-order modes, there is a risk that the MEMS device will fail to function appropriately and it might fail mechanically or electrically. We found also that locations on the PCB, other than its middle, can produce large response of the microstructure.

We investigated the effect of the electrostatic forces on the response of MEMS devices including the motion of the PCB. It was found that neglecting the PCB effect can underestimate the pull-in instability limit.

References

1. G. Li, and J. Shemansky, "Drop test analysis on micro-machined structures," *Sensors and Actuators A*, vol.85, pp.280-286, 2000.

2. V. Srikar, and S. Senturia, "The reliability of microelectromechanical systems (MEMS) in shock environments," *Journal of Microelectromechanical Systems,* vol.11, no.3, pp.206-214, 2002.

3. J. De Coster, H. Tilmans, J. Van Beek, G. Rijks, and R. Puers, "The influence of mechanical shock on the operation of electrostatically driven RF-MEMS switches," *J. Micromech. Microeng,* vol.14, no.9, pp- S49-S54, 2004.

4. T. Brown, "Harsh military environments and microelectromechanical (MEMS) devices," *Proc. of IEEE Sensors,* vol.2, pp. 753-760, 2003.

5. D. Tanner, J. Walraven, K. Helgesen, L. Irwin, N. Smith, and N. Masters, "MEMS reliability in shock environments," *Proc. IEEE Intl. Reliability Physics Symposium*, San Jose, CA, pp. 129-138, 2000.

6. X. Fang, Q. Huang, and J. Tang, "Modeling of MEMS reliability in shock environments," *Proc. of 7th Int. Conf. on Solid-State and Integrated Circuits Tech.,* Beijing, pp. 860 – 863, 2004.

7. O. Millet, D. Collard, and L. Buchaillot, "Reliability of packaged MEMS in shock environments: crack and stiction modeling," *Proc. of Design, Test, Integration and Packaging of MEMS/MOEMS,* Cannes, pp. 696 – 703, 2002.

8. J. Kimberley, R.S. Cooney, J. Lambros, I. Chasiotis, and N.S. Barker," Failure of Au RF-MEMS switches subjected to dynamic loading", *Sensors and Actuators A,* 154: pp. 140-148, 2009

9. M. Sheey, J. Punch, S. Goyal, M. Reid, M. Lishchynska, and G. Kelly, "The Failure mechanisms of micro-scale cantilevers in shock and vibration stimuli", *J. Strain,* 45(3), pp.283-294, 2009.

10. M. I. Younis, R. Miles, and D. Jordy, "Investigation of the response of microstructures under the combined effect of mechanical shock and electrostatic forces," *J. Micromech. Microeng,* vol.16, pp. 2463-2474, 2006.

11. M. I. Younis, F. M. Alsaleem, and D. Jordy, "The response of clamped-clumped microbeams under mechanical shock," *International Journal of Non-Linear Mechanics,* vol.42, pp. 643-657, 2007.

12. M. I. Younis, F. M. Alsaleem , R. Miles and Q. Su, "Characterization of the performance of capacitive switches activated by mechanical shock," *J. Micromech. Microeng*, vol. 17, pp.1360-1370, 2007.

13. M. I. Younis, D. Jordy, and J. M. Pitarresi, "Computationally efficient approaches to characterize the dynamic response of microstructures under mechanical shock," *Journal Of Microelectromechanical Systems*, vol. 16, no. 3, 2007.

14. F. M. Alsaleem, M. I. Younis, and R. Miles, "An investigation into the effect of the PCB motion on the dynamic response of MEMS devices under mechanical shock loads," *Journal of Electronic Packaging*, vol. 130, September, 2008.

15. Alsaleem, F. M., Younis, M. I, and Ibrahim, M., "A study for the effect of the PCB motion and electrostatic force on the dynamics of MEMS devices under mechanical shock," *J. Microelectromech. Syst*, Vol. 18, Issue 3, pp. 597-609, 2009.

16. M. Ibrahim and M. I. Younis, "The dynamic response of electrostatically driven resonators under mechanical shock," *J. Micromech. Microeng.*, Vol. 20, #025006, 9 pages, 2010.

17. L. Meirovitch, "Fundamentals of Vibrations," McGraw Hill, New York, (2001).

18. M. I. Younis, E. M. Abdel-Rahman, and A. H. Nayfeh, "A reduced-order model for electrically actuated microbeam-based MEMS," *J. Microelectromech. Syst.*, vol. 12, pp. 672-680, 2003.

19. E. M. Abdel-Rahman, M. I. Younis, and A. H. Nayfeh, "Characterization of the mechanical behavior of an electrically actuated microbeam." *J. Micromech. Microeng.*, vol.12, pp. 759-766, 2002.

20. F. Alsaleem, M. I. Younis, and H. M. Ouakad, "On the nonlinear resonances and dynamic pull-in of electrostatically actuated resonators." *J. Micromech. Microeng.*, vol.19, pp. 14-27, 2009.

—9—

11th. Int. Conf. on Thermal, Mechanical and Multiphysics Simulation and Experiments in Micro-Electronics and Micro-Systems, EuroSimE 2010